MANSOURA JOURNAL OF CHEMISTRY
Official Journal of Faculty of Science, Mansoura University, Egypt
E-mail: scimag@mans.edu.eg ISSN: 2974-4938

Nanometals Particles/Zeolite Modified Anode for Direct Ethanol Fuel Cells

Esraa Emara, A. M. A. OUF, A. A. Ibrahim, A. A. El-Shafei
Chemistry department, Faculty of science, Mansoura University, Egypt)
**** Correspondence to:*** *esraaemara655@gmail.com, 01063236259*

Received:10/06/2024
Accepted:10/07/2024

Abstract: Ethanol electrooxidation is crucial for fuel cells. However, a significant challenge in ethanol electrocatalysis is the breaking of the C-C bond to form CO_2 at lower overpotentials. Herein, nickel nanoparticles modified deposited on zeolite was developed for electrocatalytic oxidation of ethanol in alkaline media. The nickel modified zeolite (Ni/Z) was derived by electrodeposition method on glassy carbon (GC) at 25 °Cunder an N_2 gas. The composite possesses an efficient catalytic activity due to Ni nanoparticles have high catalytic activity, cost-effectiveness and durability. Moreover, the presence of the zeolite support accelerates the ethanol oxidation reaction (EOR) due to its high conductivity and surface area which increases the adsorption of ethanol and OH^- species at lower potentials. Using scanning electron microscopy (SEM), the as-synthesized zeolite was studied to determine the morphology structure. Cyclic voltammetry shows that EOR onset potential and current density of (Ni/20%Z/GC) electrode is strongly shifted to negative potential (E_{onset}= 0.440 V) and higher current value (I_{pa}= 26.01 mA/cm^2), respectively.

keywords: Electrochemical oxidation, Fuel cell, Transition metal ion, Zeolite.

1. Introduction

Due to the shortage of energy density of rechargeable commercial batteries,1 small fuel cell are appealing solution to the problem of providing portable energy sources. Fuel cells have been seriously considered as sources of new clean power.1,2,3 Among various types of fuel cells, direct ethanol fuel cells can compete with advanced batteries for powering portable electronic devices due to their extremely high specific energy.3 So research efforts have been devoted to finding out a cheap anode with high performance for fuel cell application. Fuel cells proved to have better conversion efficiency and reduced emissions compared to conventional alternatives. Direct alkaline alcohol fuel cells (DAAFCs) attracted growing attention over recent years. DAAFCs have favorable electro-oxidation kinetics in alkaline media, high achievable power densities, and a liquid state that is easy to handle. 2,3 Among alcohols, Ethanol emerges as a favorable option due to its lower toxicity compared to methanol and its renewable nature, derived from agricultural products and biomass fermentation. Additionally, ethanol exhibits reduced fuel crossover through the membrane and toward the oxygen electrode compared to methanol. The complete oxidation pathway of ethanol involves breaking the C-C bond and multiple dehydrogenations, presenting a significant challenge in ethanol electrocatalysis, particularly the efficient splitting of the C-C bond and oxidation to CO2 at lower overpotentials.4,5 While noble metals like Pt or Pd and their alloys are efficient catalysts,6-9 their high cost, scarcity, and susceptibility to CO poisoning limit their widespread use. As an alternative, non-precious transition metals and their derivatives have emerged as promising and cost-effective electrocatalysts for ethanol oxidation.10,11 Nickel-based electrocatalysts, in particular, have demonstrated remarkable activity and durability across various energy-related applications. Nickel electrocatalysts enhance conductivity and electronic structure, leading to increased active site density and electron transfer efficiency, thereby reducing reaction overpotential and facilitating catalytic activity.12,13,14 To address the conductivity and surface area limitations of nickel-based

catalysts, researchers have explored strategies such as incorporating electron donors (transition metal oxides) and utilizing

conducting substrates like graphite, glassy carbon, polymers, and molecular sieve zeolites. Zeolites, known for their microporous structures, offer selective ion exchange and molecular incorporation properties, making them promising candidates for electrode modification in electrocatalysis.[15-19] Herein, Ni/Z was reported as an efficient catalyst for ethanol electrochemical oxidation at lower overpotentials. Nickel-modified zeolite was synthesized by electrodeposition technique. Subsequently, the nickel was precipitated onto surface of glassy carbon (GC) by deposition of nickel chloride-zeolite at 25 °C under nitrogen gas. Scanning electron microscopy (SEM) confirmed the successful fabrication of the electrocatalysts. Various electrochemical techniques showed that the Ni/20%Z/GC electrocatalyst exhibited efficient activity for ethanol oxidation, with an onset potential of 0.440 V vs Ag/AgCl and a current density of 26.01 mA/cm². The performance is attributed to the bifunctional mechanism, where zeolite and nickel nanoparticles enhance OH^- adsorption at low potentials, promoting the formation of active sites (NiOOH).

2.Materials and procedures

2.1. Materials and chemicals

Electrolytic solutions were prepared from analytical grade chemicals, Sodium hydroxide (NaOH, Merck), absolute ethanol (C_2H_5OH, 99.99%), an Nickel chloride ($NiCl_2.6H_2O$) using distilled water produced by a Mega pure system (MP-A6 corning). Zeolite suspension was made by dispersing a defined weight of clinoptiolite zeolite (0.01, 0.02, 0.05 g) through ultrasonic vibration for 10 minutes in 6ml distilled water.

2.2. Instrumentation

Electrochemical measurements were conducted using a Versastate III conventional three-electrode cell where platinum sheet as the counter electrode and (Ag/AgCl; KCl solution of 3 M) as the reference electrode. The working electrode is the modified GCE with the prepared catalysts. Before all the electrochemical testing, the high-purity of N_2 gas was purged for 30 min.

The working electrode was 3mm glassy carbon disc (Mainland China) bound in a Teflon tube.

2.3. Electrode preparation

2.3.1. Polishing procedure

The electrode was polished on polishing cloth. The steps of polishing were follows:

a) polishing the glassy carbon electrode with µ- alumina until the surface is a mirror-like surface.

b) sonication of electrode for 10 minutes in DI water followed by acetone and left to dry.

2.3.2. Synthesis of electrocatalyts (Ni/Z)

The electrodeposition solution consists of (x mMol) $NiCl_2.6H_2O$ and (y mg) zeolite to form (Ni, 10%Z/Ni, 20%Z/Ni, 50%Z/Ni) electrodes.

2.3.3. Material Characterization

Several analysis techniques were used to characterize some of the as-synthesized samples. The morphology of nanoparticles and particle distribution was examined by scanning electron microscopy (SEM), SEM experiments were performed on a JSM-6460LV electron microscope (JEOL, Japan) operating at an accelerating voltage of 25 kV and the samples were coated with Au thin film.

2.4. Electrochemical Performances

Cyclic voltammetry (CV), Electrochemical impedance spectroscopy (EIS) and Chronoamperometry method (it-curve) were used to test the GCE modification. At a scan rate with a potential range of 0 to 0.7 V, CV tests were carried out. The first cell was employed to record the voltammogram of modified electrodes in the supporting electrolyte (NaOH), aimed at assessing the clarity of the system and characterizing these electrodes, including surface area determination. In the second cell, ethanol and NaOH were filled to evaluate the activity of the prepared electrodes towards ethanol oxidation using cyclic voltammetry and chronoamperometric techniques. Lastly, the third cell was designated for electrochemical impedance spectroscopy (EIS) measurements.

3. Results and Discussion

3.1. SEM analysis

Fig.1 (a, b) displayed the SEM images of (Ni/20%Z) and (Ni/50%Z) .respectively, The images showed the successful distribution of the nickel nanoparticles on the six prism shape glomerocryst of zeolite.[7] Fig.1a showed the SEM image of Ni/20%Z which exhibited a small particle size (uniform distribution) of Ni NPs on the zeolite surface. While the particle size of Ni NPs increased in Ni/50%Z sample (Fig.1b) indicating the growth and agglomeration of the particles.

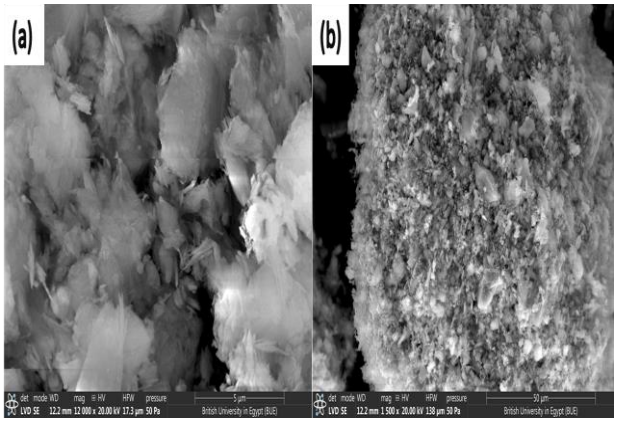

Fig.1: SEM images of (a) Ni/20%Z, (b) Ni/50%Z electrodes.

3.2. Electrochemical performance of electrocatalysts

3. 2.1. Cyclic voltammetry of anode

The electrochemical responses of Z/GC, Ni/GC, Ni/10%Z/GC, Ni/20%Z/GC, and Ni/50%Z/GC electrodes were investigated using cyclic voltammetry (CV) in a (1 M NaOH) alkaline solution within a potential range of 0 - 0.7 V. as illustrated in (Fig.2) The cyclic voltammogram indicates a lack of redox behavior for the Z/GC electrode. This can be attributed to the low conductivity and stability of zeolite. But in the case of Ni/GC, the CV displays a single pair of redox peaks (∼0.490 V oxidation and ∼0.40 V reduction) during both forward and backward scans, these peaks are associated with the adsorption of OH^- during oxidation and subsequent oxide removal during reduction. Moreover, The CV curve for Ni/10%Z/GC exhibits elevated current density, attributed to the presence of zeolite.[20,21] The zeolite increases the surface area of the electrode and enhances the conductivity of the metal oxide-supported zeolite, facilitating a uniform distribution of Ni nanoparticles on the electrode surface and consequently improving catalytic activity. With a higher percentage of zeolite (Ni/20%Z/GC), a significantly higher current density is observed in the CV, The CV curve reveals distinct redox peaks at ∼0.474 V (oxidation) and ∼0.325 V (reduction), indicating a synergistic effect between Ni oxide and zeolite, contributing to enhanced redox behavior.[21,22] The redox behavior of Ni/Z is ascribed to the oxidation and reduction of the Ni $(OH)_2$/NiOOH redox couple. Formation of Ni $(OH)_2$ Species: Ni $(OH)_2$ species are generated during Ni oxidation at lower potentials when the potential is anodically scanned in the presence of NaOH as the following equation.

$$Ni^{2+} + 2OH^- \leftrightarrow Ni(OH)_2 \quad (1)$$

$$Ni(OH)_2 + OH^- \leftrightarrow NiOOH + H_2O + e^- \quad (2)$$

As can be seen, when the percentage of zeolite material increased (20%Z), the electrochemical current of the redox activity increased because high dispersion of Ni nanoparticles can be deposited at the zeolite electrode. However, the further increase of the percentage of zeolite to 50%Z (Ni/50%Z/GC) exhibited a decrease in the electrochemical current which may be due to the agglomeration of of zeolite on surface of glassy carbon electrode; which decrease the sensitivity of the electrode response.

These findings underscore the impact of zeolite content on electrode behavior, with Ni/20%Z/GC showcasing a synergistic effect that enhances current density and redox behavior. Zeolite incorporation proves instrumental in optimizing the performance of the electrodes in an alkaline solution.

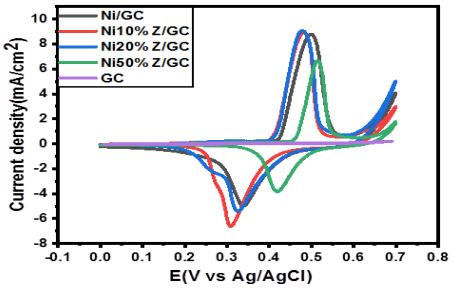

Fig.2: CVs of curves recorded in 1M NaOH at a scan rate of 50 mV s^{-1}.

3. 2.2. Effect of scan rate

Furthermore, cyclic voltammetry investigations were conducted on Ni/GC, Ni/10%Z/GC, Ni/20%Z/GC, and Ni/50%Z/GC electrodes at various scan rates ranging from 10 to 200 mV/s, within an operating voltage window of 0-0.7V. The plots depicted in Fig. 3 (a-d) illustrate that as the scan rate increased, the reduction and oxidation peaks for all electrodes shifted towards lower and higher potentials, respectively.

Because of, the oxidation peaks in the CV shift towards higher potentials with increasing scan rate. This shift is associated with quick interfacial rate kinetics. As the scan rate rises, the oxidation reactions become faster, requiring higher potentials to drive the reactions. Conversely, the reduction peaks observed in the CV move towards lower potentials. This shift is attributed to the internal resistance of the electrode. Higher scan rates lead to increased resistance within the electrode, causing the reduction reactions to occur at lower potentials

So, the overall observation of shifts in both reduction and oxidation peaks with increasing scan rate indicates that the redox processes are diffusion-controlled. This means that the rate of the redox reactions is primarily limited by the diffusion of reactants to and from the electrode surface, rather than by other factors such as reaction kinetics or mass transfer.[24]

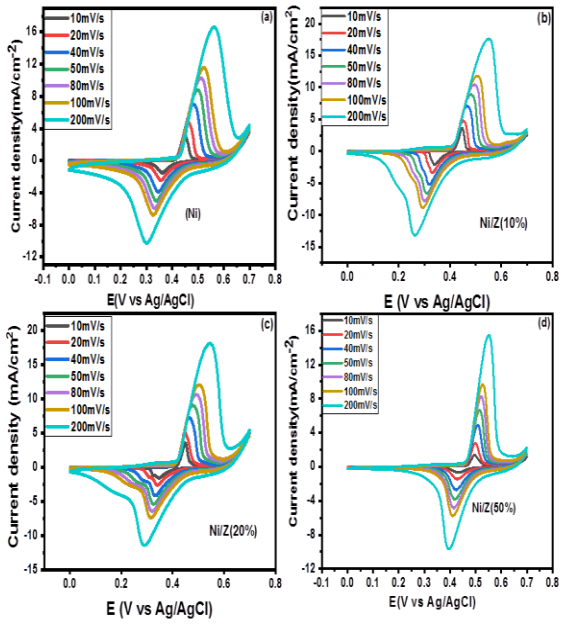

Fig.3: (a-d) effect of scan rate of prepared electrodes (10- 200 mV/s)

3.2.3. Calculation of Electrochemical Surface Area

Cyclic voltammetry (CV) was conducted over the range of 0 to 0.7 V (vs. Ag/AgCl) at a scan rate of 50 mV/s until reaching steady-state CV curves. Subsequently, CVs were executed at various scan rates from 10 to 200 mV/s under a nitrogen atmosphere, and the resultant peak current (Ipa) was plotted against the scan rate (v). The slope of this plot yields the double-layer capacitance of each electrode in farads (Cs), which is utilized to evaluate the electroactive surface area (ECSA) using the following equation.[25,26]

$$\mathbf{ECSA = C_{dl} / C_s} \qquad \mathbf{(3)}$$

Where C_{dl} (mF/cm^2) is the specific capacitance of the double layer corresponding to the material of the electrode in acidic and alkaline medium (0.035 mF/cm^2).

Through the results of the scan rate, we enable to plot a relation between the current and scan rate (Fig.4), and from the slope, we can determine the surface area, The slopes of Ni/GC, Ni/10%Z/GC, Ni/20%Z/GC and Ni/50%Z/GC precursors are 12.61, 13.12, 13.43 and 6.82 µF and from equation.1, the ECSA is found to be 0.36, 0.38, 0.38, and 0.19 cm^{-1}, respectively. It was observed that Ni/20%Z/GC exhibits the largest ECSA value compared to the other catalysts, and thus the highest catalytic activity, consistent with the CV results.

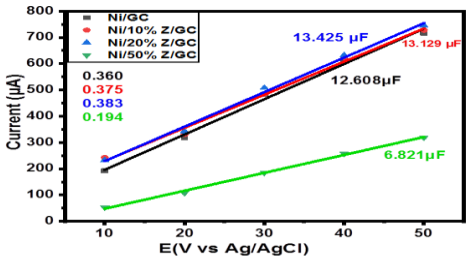

Fig.4: the corresponding linear fitting of the current density as a function of scan rates for the fabricated catalysts.

3.1.2.4. Oxidation of Ethanol (1M)

Subsequently, cyclic voltammetry (CV) was conducted at a scan rate of 50 mV s^{-1} following the introduction of 1 M ethanol, as depicted in (Fig. 5). A comparison between (Fig. 4) and the cyclic voltammogram obtained in blank NaOH (Fig. 2) reveals a significant increase in anodic

current specifically for ethanol oxidation. This pronounced rise in anodic current upon ethanol introduction indicates the occurrence of ethanol oxidation on the electrode surface, a critical step in fuel cell applications. Additionally, a cathodic peak associated with the reduction of oxy-hydroxide species is present in the figure. However, the current value of the cathodic peak is notably smaller than that of the anodic one. The relative decrease in the intensity of the cathodic peak when ethanol is introduced is attributed to the partial consumption of NiOOH (nickel oxy-hydroxide) species during ethanol oxidation. This process involves the partial consumption of NiOOH species, resulting in the formation of nickel hydroxide. The chemical reaction can be expressed as follows:[23]

$$\mathbf{NiOOH + EtOH \leftrightarrow Ni(OH)_2 + products} \quad \mathbf{(4)}$$

This reaction represents the oxidation of ethanol where nickel oxy-hydroxide (NiOOH) is partially consumed, leading to the formation of nickel hydroxide (Ni $(OH)_2$) and other products. The voltammetric analysis reveals that the zeolite ratio of 20% exhibits the most favorable electrochemical behavior. The peak height is approximately ~26.01 mA/cm². The peak potential is approximately ~0.440 V. For 10% zeolite, anodic current and onset potential are observed (~24.7 mA/cm² and ~0.450 V), respectively Due to lower amounts of the modifier reduce the extent of ion exchange. In the case of 50% of zeolite, anodic current and onset potential are observed (~18.3 mA/cm² and ~0.501 V), respectively. Due to higher amounts increase the resistance of the electrode, the sensitivity of the electrode response decreased.

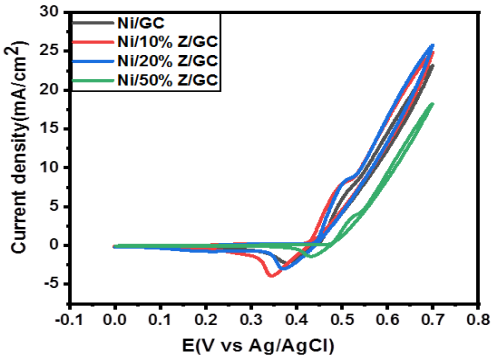

Fig.5: The effect of the zeolite ratio (a) 0 %, (b) 10%, (c) 20% and (d) 50% on the oxidation of 1 M ETOH at ZGC doped with Nickel(II) in 1 M NaOH solution at a scan rate of 50 mV s^{-1}.

3.2.5. Effect of Concentration of Ethanol

The catalytic oxidation of ethanol is influenced by its concentration, as demonstrated through the EOR tests conducted with varying ethanol concentrations. Figures 6(a-d) depict the typical CVs of Z/GC, Ni/GC, Ni/10%Z/GC, Ni/20%Z/GC, and Ni/50%Z/GC electrodes at a scan rate of 50 mVs^{-1} across different concentrations of ethanol (0.1-1M). The figures illustrate an increase in the anodic current density at higher ethanol concentrations, attributed to the adsorption of ethoxy on the catalyst surface. Additionally, the first peak corresponding to α-$Ni(OH)_2$ diminishes or disappears. This rise in oxidation current density is linked to the utilization of NiOOH during the ethanol oxidation reaction, leading to increased oxidation of β-$Ni(OH)_2$ and consequently higher current production. Moreover, the plot of ln current versus ln ethanol concentration at a specific potential (Figure 7) is utilized to estimate the reaction orders.[27]

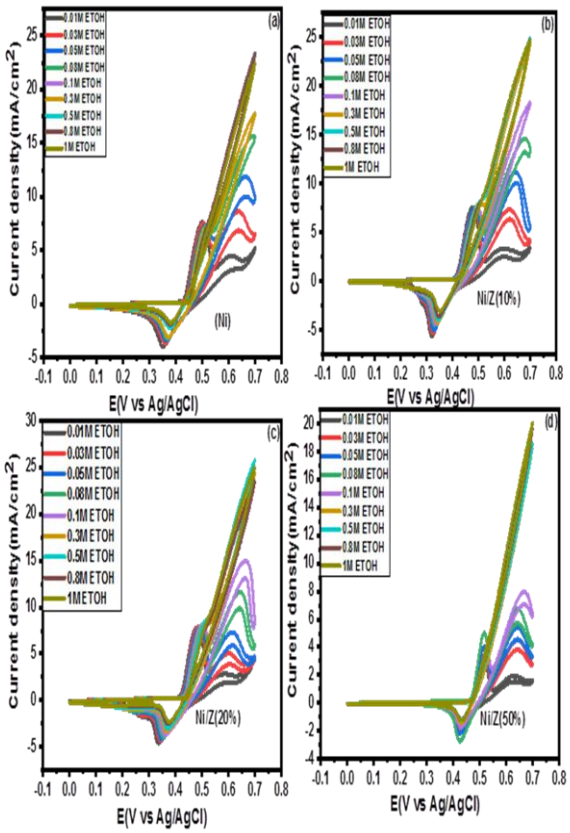

Fig.6: CV of as-prepared electrodes at (a-d) different concentrations of ethanol at 50 mV s^{-1}.

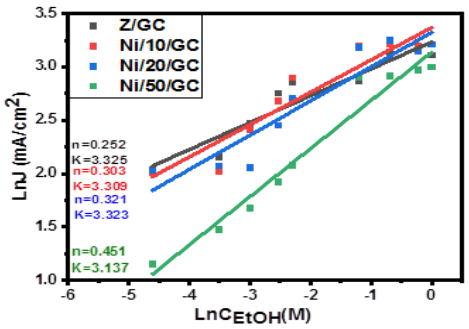

Fig.7: Plots of ln_{Jp} vs. ln $C_{ethanol}$ at constant potential obtained from 6(a-d).

3.1.2.6. Electrocatalytic oxidation of ethanol at the surface of the electrode

To delve deeper into the electrochemical oxidation mechanism of ethanol on the electrode, we examined the influence of different ethanol concentrations on cyclic voltammetric responses (Fig. 8a, 8b). In Fig. 8a, observed at low ethanol concentrations, two distinct anodic peaks, labeled as a1 (associated with the α-Ni(OH)$_2$/NiOOH couple) and a2 (related to the β-Ni(OH)$_2$/NiOOH couple), were evident. The α-Ni (OH)$_2$ form is acknowledged as unstable, initially forming during electro-oxidation and gradually converting to the more stable β-Ni(OH)$_2$.The electrode reaction corresponding to the anodic peak a2 can be expressed as follows:[28]

$$\alpha Ni(OH)_2 \xrightarrow{\text{oxidation}} \beta Ni(OH)_2 \qquad (5)$$

$$\beta Ni(OH)_2 + OH^- \leftrightarrow NiOOH + H_2O + e^- \qquad (6)$$

Therefore, the Ni (OH)$_2$ produced in reaction 3 might be β-Ni(OH)2.

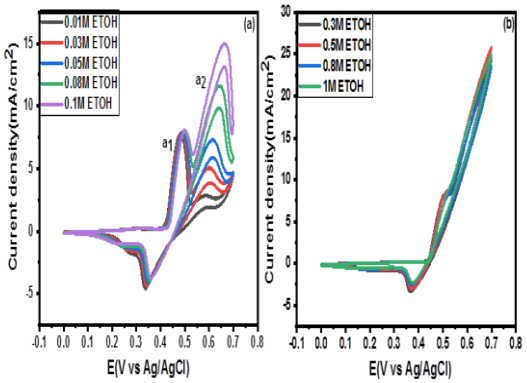

Fig.8: (a) CVs of these electrodes at low concentrations of ETOH (a) 0.01, (b) 0.03, (c) 0.05, (d) 0.08 and (f) 1M at a scan rate of 50 mVs^{-1}. (b) Cyclic voltammograms of these electrodes at high concentrations of EtOH (a) 0.3, (b) 0.5, (c) 0.8 and (d) 1M at a scan rate of 50 mV s^{-1}.

Table.1: Electrochemical analysis evaluation by cyclic voltammetry study.

	Electrochemical Surface Area (ECSA)(cm^2)	C_{dl} (µF)	E_{on} (V vs Ag/Ag Cl)	Current density (mA/cm^2)
Ni/GC	0.360	12.608	0.467	22.96
Ni/10% Z/GC	0.375	13.129	0.450	24.70
Ni/20% Z/GC	0.383	13.425	0.440	26.01
Ni/50% Z/GC	0.194	6.821	0.501	18.30

3.2.7. Electrochemical impedance spectroscopy (EIS)

Electrochemical impedance spectroscopy (EIS) was utilized to understand the electrochemical properties at the electrolyte-electrode interfaces.[29] The Nyquist plot, covering frequencies from 0.1 Hz to 105 Hz, was generated using the Randles circuit model (Fig. 9a). Each plot exhibited a semicircle in the high-frequency region and a straight line in the low-frequency region. The equivalent series resistance (Rs), representing the electrode-electrolyte interface, was determined from the left intercept of the semicircle. The charge transfer resistance (Rct) was obtained from the semicircle diameters, enabling analysis of faradic kinetics. In Fig.8a, the Ni/50%Z/GC electrode showed an Rs value of 76.4 Ω and an Rct value of 933 Ω. Comparatively, the Ni/20%Z/GC electrode had values of 100 Ω and 528 Ω, respectively. This indicates that the uniform distribution of Ni into Z/GC electrodes enhances their electrical conductivity and facilitates rapid charge transfer, promoting efficient utilization of active compounds and expedited electrochemical kinetics. Additionally, (fig.9b) illustrates the correlation between the real part of impedance (Z′) and frequency for the fabricated electrodes. It is evident from the figure that Z′ diminishes as the frequency increases across all samples. Notably, Ni/20%Z/GC exhibits the smallest magnitude value of Z′ compared to other catalysts, underscoring lower electrode interface resistances. Moreover, the diffusion kinetics were investigated through bode graphs (Fig.8c), depicting phase angle values for

Ni/GC (15°), Ni/10%Z/GC (62°), Ni/20%Z/GC (71°), and Ni/50%Z/GC (48°) electrodes at a low frequency of 10^5 Hz. Variations in the phase angle provide insights into the rate-limiting behavior, with 45° indicating a diffusion-limited response and 90° reflecting a completely capacitive response. The angles for Ni/GC, Ni/50%Z/GC and Ni/10%Z/GC are closer to 45°, signifying a dominant diffusion-controlled mechanism. Conversely, with the best percent of zeolite, the angle for Ni/20%Z/GC increased to 71°, approaching the

ideal capacitor value of 90°. This reaffirms the surface capacitive properties of Ni/20%Z/GC nanocomposites.

Finally, in Fig. 9d, a linear relationship is depicted between the real part of the impedance (Zre) and the reciprocal of the square root of the angular frequency (ω-1/2) in the low-frequency region. This relationship is useful for investigating the conductivity of electrodes and calculating the diffusion coefficient (D) of the OH- species using the following equations:[30]

$$\mathbf{Zre = Rct + Rs + \sigma\omega^{-1/2}} \qquad \mathbf{(7)}$$

$$\mathbf{D = R^2T^2 / (2\,A^2F^4C^2n^4\sigma^2)} \qquad \mathbf{(8)}$$

Where Rct, Rs, and σ represent the charge transfer resistance, inner resistance, and Warburg factor (the slope of the linear relationship in Fig. 8d), respectively. Additionally, R, T, F, n, A and C denote the ideal gas constant (8.314 J/mol/K), the absolute temperature (K), the Faraday constant (96,486 C/mol), the number of electrons per molecule, the surface area of the GC electrode (0.0706 cm²), and the concentration of the ions (1 x 10^{-3} mol cm^{-3}), respectively.[31] Consequently, the diffusion coefficient (D) value of the Ni/20%Z/GC electrode is approximately 6.60 x 10^{-10} cm²/s, which surpasses that of Ni/GC (1.43 x 10^{-11} cm²/s), Ni/10%Z/GC (1.39 x 10^{-12} cm²/s), and Ni/50%Z/GC (4.46 x 10^{-12} cm²/s).

Table. 2: Comparison list of EIS parameters of the fabricated catalysts for the EOR.

Sample	Rs (Ω)	Rct (Ω)	θ (deg)
Ni/GC	**88.9**	**809.9**	15
Ni/10%Z/GC	**84.3**	**605**	62
Ni/20%Z/GC	**100**	**528**	71
Ni/50%Z/GC	76.4	933	48

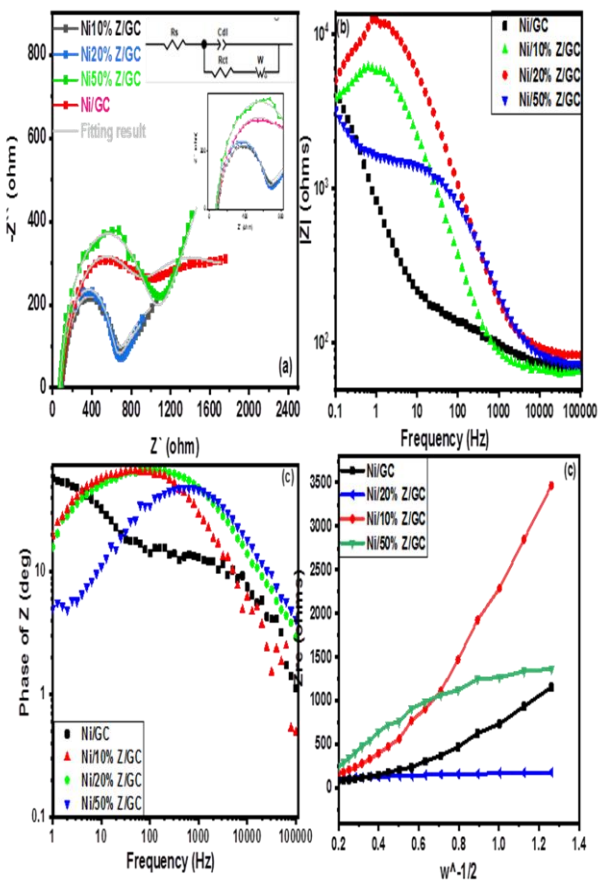

Fig.9: (a) The EIS plots of the as-prepared catalysts at E= 0.4 V vs Ag/AgCl and an amplitude of 5 mV in 1M NaOH+ 1M ETOH solution, (b) Bode plots for all catalysts, (c) The frequency-dependent real part of the impedance, and (d) the linear relationship of Zre vs. $\omega^{-1/2}$.

3. 2.8. Stability of electrocatalysts

Finally, stability and durability (Fig.10) were other targets for fabricating electrocatalysts to achieve high and long-time electrocatalytic performance. The stability of prepared catalysts was investigated by chronoamperometric analysis (I-t curve) which was measured in NaOH (1 M) in presence of ethanol (1 M) at fixed potential 0.6 V (vs Ag/AgCl) at room temperature. According to the chronoamperogram (I-t curve), the initial drop in current densities of prepared catalysts is followed by stability decay.[32] As observed in Fig.9, the Ni/20%Z/GC catalyst was more stable and gives higher current density than those of other electrodes.

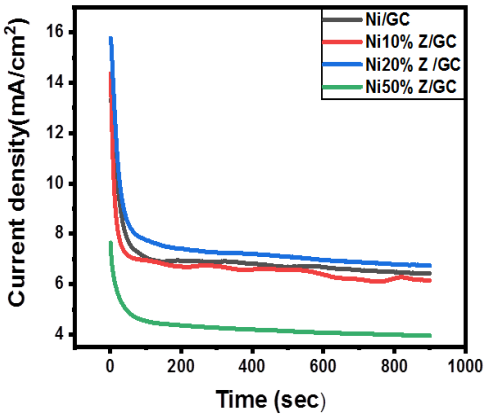

Fig.10: I-t curve measurements in NaOH (1 M) in presence of ethanol (1 M) at fixed potential 0.6 V (vs Ag/AgCl) at room temperature.

5. Conclusion

In summary, Modifying zeolite to Ni deposited zeolite (Ni/Z) proves to be a promising strategy for creating highly efficient electrocatalysts for ethanol oxidation reaction (EOR).The nickel modified zeolite (Ni/20%Z/GC) was derived by electrodeposition method on glassy carbon (GC) at 25 ℃ under an N_2 gas. Electrochemical kinetics were evaluated using cyclic voltammetry (CV) in 1 M NaOH at a scan rate of 50 mV/s within the potential range of 0 to 0.7 V (vs. Ag/AgCl). The CV curves illustrate a notable shift in the EOR onset potential and current density towards negative potential and higher current values, respectively, compared to other electrodes. This shift is attributed to the formation of functional materials, which provide a higher number of active sites for the reaction. Additionally, the current density increased proportionally with scan rate, indicating good electrochemical stability of the fabricated materials. Furthermore, the electrocatalytic activity of the nanocomposites for EOR was assessed across various ethanol concentrations (0.01-1M), revealing an increase in current density with higher ethanol concentrations, signifying enhanced ethanol electrooxidation. Moreover, the catalyst demonstrated superior stability compared to other electrodes. Overall, this study underscores the potential of fabricating highly efficient and stable zeolite-derived catalysts for EOR applications utilizing non-precious-based materials.

Reference

1. Mohammadi, T.; Hosseini, M. G.; Ashassi-Sorkhabi, H.; Sefidi, P. Y., (2023) Investigating performance of flower-like CoCu-MOF supported on carbon felt as a binder-free anode electrode in direct ethanol fuel cell. Synth Met, 298, 117443.
2. Zhou, W.; Gao, L.; Zhang, Y.; Hu, T., (2021) Composites of Ni-MOF and polyaniline hydrogel for carbon monoxide resistant excellent catalysts of ethanol oxidation reaction. *Int J Hydrogen Energy*, **46 (53)**, 27128-27137.
3. Chen, Y.; Wen, Y.; Zhou, Q.; Shen, L.; Du, F.; Peng, P.; Chen, Y.; Zheng, J., (2023) Electrochemically-induced highly reactive PdO* interface on modulated mesoporous MOF-derived Co3O4 support for selective ethanol electro-oxidation. *Journal of Energy Chemistry*.
4. Shang, Q.; Hu, L.; Hu, Y.; Liu, C.; Zhou, Y., (2018) Fabrication of superhydrophobic fluorinated silica nanoparticles for multifunctional liquid marbles. Appl. Phys. A, 124 (1), 25.
5. Wang, Q.; Duan, J. D.; Goetjen, T.; Hupp, J.; Notestein, J., (2023) Bimetallic NiCu catalysts supported on a Metal-Organic framework for Non-oxidative ethanol dehydrogenation. *J Catal*, **422**, 86-98.
6. Moraes, L. P. R.; Matos, B. R.; Radtke, C.; Santiago, E. I.; Fonseca, F. C.; Amico, S. C.; Malfatti, C. F., (2016) Synthesis and performance of palladium-based electrocatalysts in alkaline direct ethanol fuel cell. *Int J Hydrogen Energy*, **41 (15)**, 6457-6468.
7. Li, Y.; Sun, H.; Feng, R.; Wang, Y.; Subhan, F.; Yan, Z.; Zhang, Z.; Liu, Z., (2015) Synthesis of ZSM-5 zeolite from diatomite for fluid catalytic cracking (FCC) application. Appl Petrochem Res, **5 (4)**, 347-353.
8 Moraes, L. P. R.; Matos, B. R.; Radtke, C.; Santiago, E. I.; Fonseca, F. C.; Amico, S. C.;Malfatti, C. F., (2016) Synthesis and performance of palladium-based electrocatalysts in alkaline direct ethanol fuel cell. *Int J Hydrogen Energy*, **41 (15)**, 6457-6468.

9 Askari, M. B.; Salarizadeh, P.; Seifi, M.; Rozati, S. M., (2019) Ni/NiO coated on multi-walled carbon nanotubes as a promising electrode for methanol electro-oxidation reaction in direct methanol fuel cell. Solid State Sciences**,97**, 106012.

10. Gamal, S.; Kospa, D. A.; Gebreil, A.; El-Hakam, S. A.; Ahmed, A. I.; Ibrahim, A. A., (2023).NiCo2O4 spinel supported N-dopped porous Hollow carbon derived MOF functionalized SiO2 for efficient ORR electrocatalysis. *Int J Hydrogen Energy*

11 Vyas, A. N.; Saratale, G. D.; Sartale, S. D., (2020) Recent developments in nickel based electrocatalysts for ethanol electrooxidation. *Int J Hydrogen Energy*, **45 (10)**, 5928-5947.

12 Tan, D.; Cui, C.; Shi, J.; Luo, Z.; Zhang, B.; Tan, X.; Han, B.; Zheng, L.; Zhang, J.; Zhang, J., (2019) Nitrogen-carbon layer coated nickel nanoparticles for efficient electrocatalytic reduction of carbon dioxide. Nano Res, **12 (5)**, 1167-1172.

13 Zhou, L.; Qu, Z.; Fu, L., (2023) ,Rational design of hollow nitrogen-doped carbon supported nickel nanoparticles for efficient electrocatalytic CO2 reduction. *Journal of Environmental Chemical Engineering* **11 (2)**, 109427.

14. Abbas, S. A.; Iqbal, M. I.; Kim, S.-H.; Abbas Khan, H.; Jung, K.-D., Facile (2019) synthesis of alfa-nickel hydroxide by an ultrasound-assisted method and its application in energy storage devices. Appl Surf Sci, 218-226.

15 Ichikawa M (2000) Platin Met Rev 44:3

16 Bedioui F, Roué L, Briot E, Devynck J (1994) *J Electroanal Chem* 373:19

17. Ozin GA, Kuperman A, Stein A (1989) Angew Chem Int Ed Engl 28:359

18 Rolison DR (1990) Chem Rev 90:867

19. Bard AJ, Mallouk TE (1992) In: Murray RW (ed) Molecular design of electrode surfaces. Wiley, New York, p 271

20. Mohan, N.; Cindrella, L., (2017) Template-free synthesis of Pt-MOx (M = Ni, Co & Ce) supported on cubic zeolite-A and their catalytic role in methanol oxidation and oxygen reduction reactions characterized by the hydrodynamic study. *Int J Hydrogen Energy*,**42 (34)**, 21719-21731.

21. Sancho, T.; Lemus, J.; Urbiztondo, M.; Soler, J.; Pina, M. P.,(2008) Zeolites and zeotype materials as efficient barriers for methanol cross-over in DMFCs. Micropor Mesopor Mat, **115** (1-2), 206-213.

22. Hosseini, M. G.; Momeni, M. M.; Faraji, M., (2019) Highly active nickel nanoparticles supported on tio2 nanotube electrodes for m 23.Hassanzadeh, V.; Sheikh-Mohseni, M. A.; Habibi, B., Catalytic oxidation of ethanol by a nanostructured Ni-Co/RGO composite: Electrochemical construction and investigation. *Journal of Electroanalytical Chemistry*, 847, 113200.

23 ethanol electrooxidation. Electroanalysis (2010), 22 (22), 2620-2625.

24 Soliman Gamal, Doaa A. Kospa, Amr Awad Ibrahim, Awad I. Ahmed, A. M. A. Ouf. (2024) " A comparative study of α-Ni(OH) and Ni nanoparticle supported ZIF-8@reduced graphene oxide-derived nitrogen doped carbon for electrocatalytic ethanol oxidation " , RSC Advances,

25 Gamal, S.; Kospa, D. A.; Gebreil, A.; El-Hakam, S. A.; Ahmed, A. I.; Ibrahim, A. A., (2023).NiCo2O4 spinel supported N-dopped porous Hollow carbon derived MOF functionalized SiO2 for efficient ORR electrocatalysis. *Int J Hydrogen Energy*

26 Gamal, S.; Kospa, D. A.; Kaid, M. M.; El-Hakam, S. A.; Ahmed, A. I.; Ibrahim, A. A., (2023) Fe-Co spinel oxides supported UiO-66-NH2 derived zirconia/ N-dopped porous hollow carbon as an efficient oxygen reduction reaction electrocatalyst. *Journal of Environmental Chemical Engineering*, **11 (2)**, 109359.

27 Youssef, A. M.; Ahmed, A. I.; Amin, M. I.; El-Banna, U. A., (2014) Adsorption of lead by activated carbon developed from rice husk. Desalination Water Treat, 1-14.

28 Subbaiah, T.; Mallick, S. C.; Mishra, K. G.; Sanjay, K.; Das, R. P., (2002) Electrochemical precipitation of nickel hydroxide. *J Power Sources*, **112 (2)**, 562-569.

29 Rahmani, K.; Habibi, B., (2019) NiCo alloy nanoparticles electrodeposited on an

electrochemically reduced nitrogen-doped graphene oxide/carbon-ceramic electrode: a low cost electrocatalyst towards methanol and ethanol oxidation. RSC Adv, **9 (58)**, 34050-34064.

30 Lan, J.; Hou, H.; Huang, B.; Li, H.; Li, J., (2022) The positive role of vitamin C in spindle-like LiFePO4/C cathode derived from two wastes. Ionics (Kiel), **28 (4)**, 1583-1593.

31 Ghanem, R. M.; Kospa, D. A.; Ahmed, A. I.; Ibrahim, A. A.; Gebreil, A., (2023) Construction of thickness-controllable bimetallic sulfides/reduced graphene oxide as a binder-free positive electrode for hybrid supercapacitors. RSC Adv, **13 (42)**, 29252-29269.

32 Rahmani, K.; Habibi, B., (2019) NiCo alloy nanoparticles electrodeposited on an electrochemically reduced nitrogen-doped graphene oxide/carbon-ceramic electrode: a low cost electrocatalyst towards methanol and ethanol oxidation. RSC Adv, **9 (58)**, 34050-34064.